'This is the peer reviewed version of the following article: Badaruddin, S., Werner, A. D., & Morgan, L. K. (2017). Characteristics of active seawater intrusion. Journal of Hydrology, 551, 632–647. https://doi.org/10.1016/j.jhydrol.2017.04.031

which has been published in final form at http://doi.org/10.1016/j.jhydrol.2017.04.031

Characteristics of active seawater intrusion

Sugiarto Badaruddin[2,3], Adrian D. Werner[1,2*], Leanne K. Morgan[2,4]

[1]National Centre for Groundwater Research & Training, Flinders University, GPO Box 2100, Adelaide SA 5001, Australia

[2]School of the Environment, Flinders University, GPO Box 2100, Adelaide SA 5001, Australia

[3]Civil Engineering Department, the State Polytechnic of Ujung Pandang, P.O. Box 90245, South Sulawesi, Indonesia

[4]Waterways Centre for Freshwater Management, University of Canterbury and Lincoln University, Private Bag 4800, Christchurch 8140, New Zealand

Email addresses:

Sugiarto Badaruddin: sugi0040@flinders.edu.au

*Adrian D. Werner: adrian.werner@flinders.edu.au; Corresponding author

Leanne K. Morgan: leanne.morgan@canterbury.ac.nz

Resubmitted to Journal of Hydrology, 31st March 2017

Abstract

The inland migration of seawater in coastal aquifers, known as seawater intrusion (SWI), can be categorised as passive or active, depending on whether the hydraulic gradient slopes downwards towards the sea or the land, respectively. Despite active SWI occurring in many locations, it has received considerably less attention than passive SWI. In this study, active SWI caused by an inland freshwater head decline (FHD) is characterised using numerical modelling of various idealised unconfined coastal aquifer settings. Relationships between key features of active SWI (e.g., interface characteristics and SWI response time-scales) and the parameters of the problem (e.g., inland FHD, freshwater-seawater density contrast, dispersivity, hydraulic conductivity, porosity and aquifer thickness) are explored for the first time. Sensitivity analyses show that the SWI response time-scales under active SWI situations are influenced by both the initial and final boundary head differences. The interface is found to be steeper under stronger advection (i.e., caused by the inland FHD), higher dispersivity and hydraulic conductivity, and lower aquifer thickness, seawater density and porosity. The interface movement is faster and the mixing zone is wider with larger hydraulic conductivity, seawater-freshwater density difference, and aquifer thickness, and with lower porosity. Dimensionless parameters (Peclet number and mixed convection ratio) from previous steady-state analyses offer only limited application to the controlling factors of passive SWI, and are not applicable to active SWI. The current study of active SWI highlights important functional relationships that improve the general understanding of SWI, which has otherwise been founded primarily on steady-state and passive SWI.

Keywords: Seawater intrusion, density-dependent flow, solute transport, coastal aquifer, buoyancy

1. Introduction

Seawater intrusion (SWI) is a phenomenon where seawater displaces fresh groundwater in coastal aquifers (Bear, 1979). The global significance of SWI is well-established (Wu et al., 1993; Bocanegra et al., 2010; Custodio, 2010; Werner et al., 2013b). Previous studies have recognized two types of SWI: passive and active (Mahesha, 1995; Morgan et al., 2012; Werner et al., 2012). In passive SWI, the hydraulic gradient slopes towards the sea. This results in density-induced forces acting in the opposite direction to fresh groundwater flow, creating the classical wedge-shaped seawater plumes that are traditionally associated with SWI (e.g., Pinder and Cooper, 1970). In active SWI, the hydraulic gradient slopes towards the land, and forces caused by density differences and fresh groundwater flow act in the same direction, causing more aggressive salinization.

The current understanding of SWI is based primarily on studies that assume a steady-state condition (Werner et al., 2013a). For example, a considerable body of SWI research adopts the Henry problem (Henry, 1964), and modifications thereof, to investigate the effects of density, heterogeneities and dispersion on steady-state SWI (e.g., Simpson and Clement, 2003; Held et al., 2005; Abarca et al., 2007; Sebben et al., 2015). Several studies use the shift in the interface between one steady-state condition and another in evaluating long-term extents of SWI (e.g., Werner and Simmons, 2009; Morgan et al., 2012), thereby neglecting altogether transient effects and precluding the evaluation of active SWI processes. Morgan et al. (2012) showed that if the freshwater-saltwater interface moves slowly enough, steady-state solutions reproduce approximately the transient interface. This permits use of quasi-equilibrium predictions of the transient interface, thereby avoiding the numerical burden of transient analyses.

Previous studies of the transience of SWI have mainly considered passive SWI (e.g., Chang et al., 2011; Webb and Howard, 2011; Morgan et al., 2015). For example, Watson et al. (2010) investigated transient SWI in response to both sea-level rise (SLR) and sea-level drop in unconfined coastal aquifers, and defined a SWI response time-scale as the time needed for the freshwater-saltwater interface toe (i.e., the inland limit of the saltwater wedge along the aquifer basement) to reach 95% of the new steady-state condition. They observed temporal asymmetry in the SWI responses to rises and falls in sea level, and discovered the phenomenon known as 'SWI overshoot' (e.g., Morgan et al., 2013c). Following Watson et al. (2010), Lu and Werner (2013) employed the same definition of SWI time-scales in their investigation of response times associated with passive SWI, created by variations in the inland or coastal water level. They showed that for a particular coastal aquifer, the SWI response time-scale is determined by the final boundary head difference (i.e., the difference between inland and coastal boundary heads after an inland freshwater head decline (FHD)), regardless of the toe response distance associated with particular FHD events. In contrast, the toe response distance controls the time-scale of seawater retreat for cases with the same initial boundary head differences.

Compared to passive SWI, active SWI has received considerably less research attention, and general intuition about the controlling factors and time-scales of active SWI is under-developed, despite that active SWI is known to occur in many areas (i.e., Yakirevich et al., 1998; Fetter, 2001; Werner and Gallagher, 2006; Morgan and Werner, 2015). A prominent case study of active seawater intrusion is Vázquez-Suñé et al.'s (2006) investigation of the Llobregat Delta (Spain), where groundwater levels fell to more than 25 m below sea level in the 1970s, creating active SWI conditions that led to rapid and extensive salinization of the coastal aquifers. Studies of the processes accompanying active SWI include that of Badaruddin et al. (2015), who used physical and numerical modelling to show that under active SWI conditions and in the absence of recharge, the potential for watertable salinization (WTS) was significant for non-tidal unconfined coastal aquifers. The transition from passive to active SWI, which is accompanied by cessation of fresh groundwater discharge to the sea, leads to WTS arising from the landward flow of seawater. WTS may occur at rates up to, or temporarily faster than, the speed of SWI along the aquifer base (Badaruddin et al., 2015). SWI causes more extensive WTS in tidal settings relative to non-tidal conditions (Werner and Lockington, 2006). Active SWI is largely an unstudied phenomenon from the perspective of its primary characteristics and key controlling forces. Thus, intuition on the behaviour of active SWI is based largely on case studies, where the individual contributions of buoyancy, dispersive and advective forces to aquifer salinization are not investigated. The studies by Werner and Lockington (2006) and Badaruddin et al. (2015) did not explore the key features of active SWI and their relationships with the main system parameters, and rather, they focused on tidal effects and WTS, respectively.

This study investigates the characteristics of transient, active SWI occurring in cross section in various non-tidal, unconfined coastal aquifer settings, which are homogeneous, of simple geometry, and devoid of surface recharge. For the purpose of comparison, passive SWI conditions are also considered. Research by Badaruddin et al. (2015) and Abarca et al. (2004; 2007), who provide general guidance on steady-state SWI, are extended in this study by attempts to draw relationships between key features of active SWI (e.g., interface slope, mixing zone width and SWI time-scales) and the main controlling forces (e.g., density, dispersion and advection). We also extend the passive SWI characterisation of Lu and Werner (2013) using a modification to their approach to quantify active SWI time-scales.

2. Methodology

2.1. Conceptual model

Figure 1 shows a schematic representation of a simple unconfined coastal aquifer, and identifies the key parameters adopted in quantifying the main features of active SWI. The analysis applies to unconfined aquifers because these more often support freshwater extraction given their shallow occurrence relative to confined systems (Watson et al., 2010; Werner et al., 2013b).

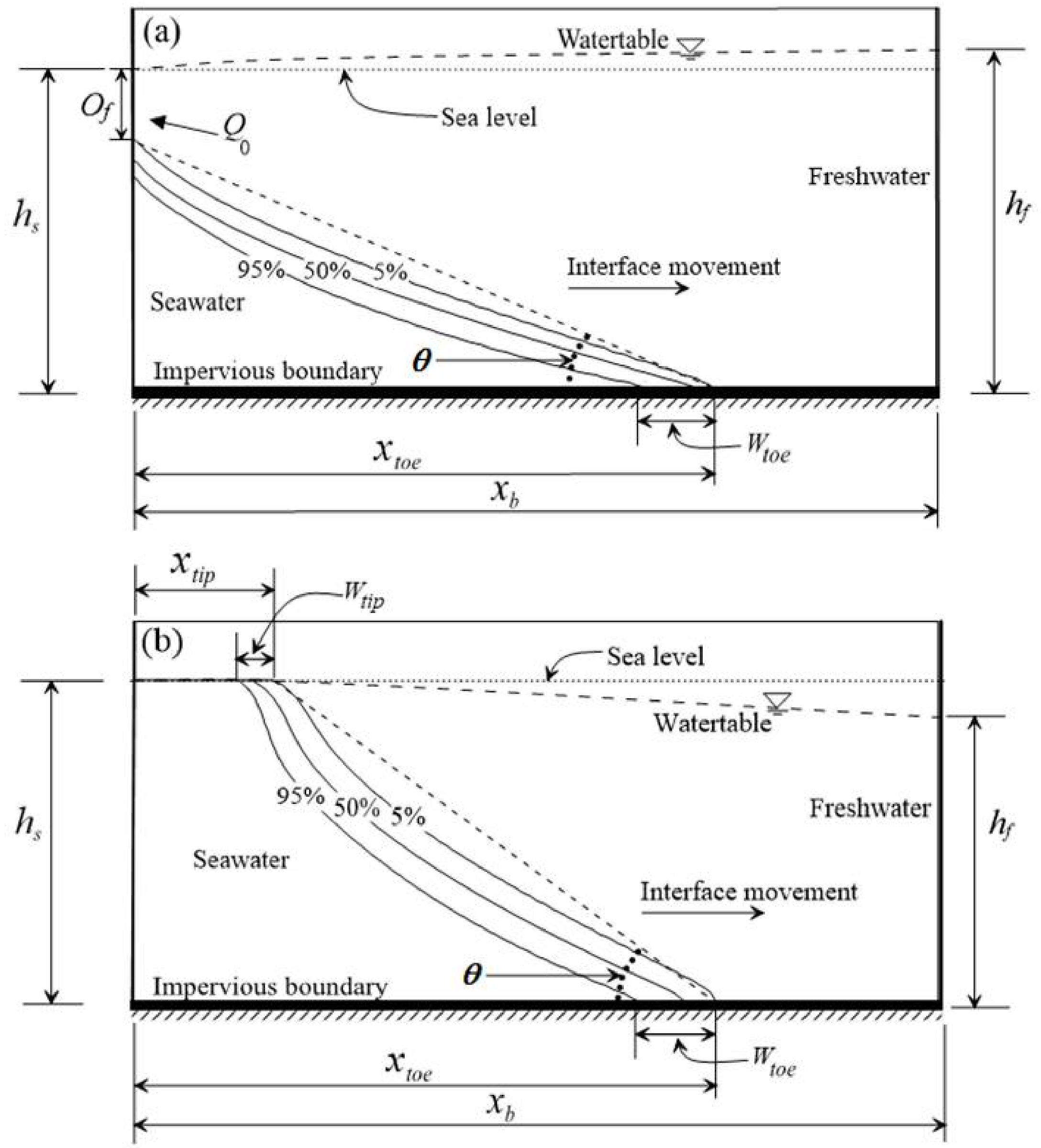

Figure 1. Conceptual model of an unconfined coastal aquifer subjected to: (a) passive SWI and (b) active SWI (modified after Badaruddin et al., 2015).

The left and the right sides of the conceptual model (Figure 1) are the coastal and inland boundaries, respectively. Q_0 [L^2/T] is freshwater discharge to the sea, and O_f [L] is the depth of freshwater discharging at the shoreline (i.e., 'outflow face'), which is shown in Figure 1 as the distance from the watertable to the 5% relative salinity on the ocean boundary. Obviously, O_f is dependent on the choice of relative salinity value used to define 'freshwater'. The regional head difference ($h_{f\text{-}s}$ [L]) is the advective force driving groundwater flow between the boundaries, and is represented by $h_f - h_s$, where h_s [L] is the depth of the horizontal aquifer base below sea level, and h_f [L] is the inland freshwater head (Figure 1). Surface recharge is neglected for simplicity. Recharge creates a mitigating effect on watertable salinization during active SWI, as shown by Werner (2017), and therefore, the results of the analysis that follows may overestimate the watertable salinization that is likely to occur in regions that experience persistent, significant recharge. Three different salinity values (i.e., 5%, 50% and 95% of seawater, termed 'relative salinity' in what follows) provide the basis for evaluating the behaviour of the interface, and both the interface toe (x_{toe} [L]) and the interface tip (x_{tip} [L]) are reported (Figure 1). The horizontal length between the 5% and 95% relative salinity contours is adopted as the width of the dispersion zone, which is calculated both at the interface toe (W_{toe} [L]) and at the watertable (i.e., the interface tip) (W_{tip} [L]). The interface slope (θ) is obtained from a straight line connecting the interface toe and tip.

A number of relationships between key hydrogeological parameters and the nature of active SWI are expected based on direct application of Darcy's Law, and given studies by Lu and Werner (2013) and Badaruddin et al. (2015). For example, the interface will migrate faster with higher hydraulic conductivity (K), lower effective porosity (n), steeper hydraulic gradient and greater density difference between freshwater and seawater. In addition, the mixing zone will be wider in models that adopt higher values of dispersion parameters. However, other aspects of active SWI behaviour remain unclear, including links between density differences and the mixing zone width, relationships between time-scales and parameter combinations, and the factors that control the steepness of the interface during active SWI. More generally, investigation is warranted of the relative contributions of advective, dispersion and buoyancy forces in controlling the nature of active SWI.

The approach to modelling SWI is similar to numerical experiments by Lu and Werner (2013), whereby the initial interface position represents the steady-state condition, and then an instantaneous inland FHD of Δh_f [L] causes the interface to move landward. Under active SWI, there is no final steady-state condition, because the interface toe eventually intrudes to the inland boundary, unlike passive SWI, in which seawater eventually restabilises to a new location. On the basis of sharp-interface theory, SWI will reach the inland boundary unless h_f exceeds the equivalent freshwater head at the base of the coastal boundary (h_{base}) (Werner et al., 2012). Here, $h_{base} = h_s \rho_s / \rho_f$, where ρ_s [M/L^3] is saltwater density and ρ_f [M/L^3] is freshwater density. Active SWI occurs if $h_f < h_{base}$.

The aquifer properties of the base case reflect those used by Lu and Werner (2013). That is, the coastal aquifer is homogeneous and isotropic, K is 10 m/d, n is 0.3, specific yield is 0.25, distance to the inland specified-head boundary (x_b) is 1000 m and h_s is 30 m. The values of ρ_s and ρ_f are 1025 kg/m^3 and 1000 kg/m^3, respectively. The longitudinal dispersivity (α_L) is 1 m and the transverse dispersivity (α_T) is one tenth of α_L (Lu and Werner, 2013; Abarca et al., 2007). Molecular diffusion (D_m) is 8.64×10^{-5} m^2/d.

The behaviour of the interface under various hydrogeological conditions and rates of passive and active SWI was explored primarily using sensitivity analysis. Table 1 outlines the various cases, which encompass several values of the final boundary head difference ($h'_{f\text{-}s}$) (i.e., after FHD), K, α_L, n, ρ_s and h_s, resulting in 64 SWI cases at the 1-km scale. Negative values of $h'_{f\text{-}s}$ indicate a lower h_f relative to h_s (Table 1, Figure 1). A field-scale case, i.e., using parameters typical of the Pioneer Valley aquifer, Australia (Case 65) (Werner and Gallagher, 2006) is included. Cases 1 ($h'_{f\text{-}s}$ = 1 m) and 3 ($h'_{f\text{-}s}$ = -1 m) are the passive and active SWI base cases, respectively. In Table 1, Cases 1, 5, 9, … 41 represent passive SWI, and the other cases involve active SWI. We use a similar method to that adopted by Lu and Werner (2013) to seek empirical relationships between SWI response time-scales and the inland FHD.

Table 1. Parameter values for SWI cases.

Case	Initial h_f	Post-FHD h_f	FHD Δh_f	h_s	$h'_{f\text{-}s}$	x_b	K	n	α_L	ρ_s
	M	m	m	m	m	m	m/d	-	m	kg/m^3
1 to 4	32	31 to 28	1 to 4	30	1 to -2	1000	10	0.30	1	1025
5 to 8	32	31 to 28	1 to 4	30	1 to -2	1000	5	0.30	1	1025
9 to 12	32	31 to 28	1 to 4	30	1 to -2	1000	20	0.30	1	1025
13 to 16	32	31 to 28	1 to 4	30	1 to -2	1000	10	0.30	0.1	1025
17 to 20	32	31 to 28	1 to 4	30	1 to -2	1000	10	0.30	10	1025
21 to 24	32	31 to 28	1 to 4	30	1 to -2	1000	10	0.30	1	1020
25 to 28	32	31 to 28	1 to 4	30	1 to -2	1000	10	0.30	1	1030
29 to 32	28	27 to 24	1 to 4	26	1 to -2	1000	10	0.30	1	1025
33 to 36	36	35 to 32	1 to 4	34	1 to -2	1000	10	0.30	1	1025
37 to 40	32	31 to 28	1 to 4	30	1 to -2	1000	10	0.25	1	1025
41 to 44	32	31 to 28	1 to 4	30	1 to -2	1000	10	0.35	1	1025
45	31.5	29.5	2	30	-0.5	1000	10	0.30	1	1025
46	32.5	30.5	2	30	0.5	1000	10	0.30	1	1025
47 to 50	33 to 31.5	30.5 to 29	2.5	30	0.5 to -1	1000	10	0.30	1	1025
51	31.5	28.5	3	30	-1.5	1000	10	0.30	1	1025
52 to 54	33.5 to 32.5	30.5 to 29.5	3	30	0.5 to -0.5	1000	10	0.30	1	1025
55	31.5	28	3.5	30	-2	1000	10	0.30	1	1025
56 to 59	34 to 32.5	30.5 to 29	3.5	30	0.5 to -1	1000	10	0.30	1	1025
60 to 64	34.5 to 32.5	30.5 to 28.5	4	30	0.5 to -1.5	1000	10	0.30	1	1025
65	41.6	36.2	5.4	37	-0.8	4750	166	0.10	10	1025

2.2. Numerical model

The variable-density groundwater flow and transport code SEAWAT version 4 (Langevin et al., 2008) was used to conduct numerical experiments of SWI in two-dimensional cross-sections. SEAWAT is widely applied, and has been tested against several benchmark problems (e.g., Langevin et al., 2003; Brovelli et al., 2007; Goswami and Clement, 2007). The governing equations and the numerical implementation of SEAWAT are given in the user manual (e.g., Langevin et al., 2008), and are therefore not shown here for brevity.

The base case model domain is 35 m high and 1000 m long. The mesh Peclet number (Pe_m [-]) suggested by Voss and Souza (1987) was used in specifying the discretization of the model domain:

$$Pe_m = \frac{\Delta L}{\alpha_L} < 4 \tag{1}$$

where ΔL [L] is the grid spacing. Initially, a uniform grid size of Δx = 1.0 m and Δz = 0.5 m was used, resulting in a grid of 70,000 cells and a Pe_m of 1. A grid-dependence test was conducted using both passive and active SWI base cases, and considering alternative levels of discretization, namely (Δx, Δz) equal to (0.5 m, 0.5 m), (0.5 m, 0.25 m) and (2 m, 1 m). The simulation results showed differences of less than 1% in the transient interface locations between the initial grid spacing and finer grids, and more than 5% compared to the coarser grid model. Therefore, the initial grid spacing (1.0 m, 0.5 m) was adopted in this study. For Case 65 (the field case), the domain height was 47 m, and a uniform grid size of Δx = 10 m and Δz = 0.5 m (i.e., Pe_m = 1) was applied.

The left and right boundaries of the model (Figure 1) represent seawater and freshwater hydrostatic conditions, respectively, defined by specified-head boundary conditions. The solute boundary condition at the coastal boundary is one where inflowing water has the concentration of seawater, whereas outflowing water is assigned the ambient concentration of groundwater at the boundary. The base of the domain is a no-flow condition. The initial steady-state condition (pre-FHD) was obtained by running transient simulations for 150 y, by which time no change was observed in salinity distributions in all cases. Instantaneous inland FHD simulations were conducted using SEAWAT's CHD package (Langevin et al., 2003), which was assigned only to the part of the inland boundary that remained fully saturated after the FHD.

2.3. Dimensionless ratios in passive and active SWI

The primary controlling factors that affect transient interface behaviour in SWI problems include buoyancy forces (i.e., water density variations), advective forces (i.e., resulting from boundary head differences) and dispersion (Goswami and Clement, 2007; Werner et al., 2013a). Abarca et al. (2004; 2007) used Henry's (1964) dimensionless parameters, which we refer to as mixed-convection ratio (*MCR*) and Peclet number (*Pe*), to characterise mixed-convective (i.e., hydraulically driven versus density-driven convection) and advective-dispersive processes, respectively, in the steady-state Henry problem. *MCR* is defined as:

$$MCR = \frac{q_f}{K\delta} \qquad (2)$$

where δ [-] is dimensionless buoyancy, calculated as $\delta = (\rho_s - \rho_f)/\rho_f$, and q_f [L/T] is the freshwater Darcy velocity ($q_f = Q_f/h_f$). Q_f [L^2/T] is freshwater flow at the inland boundary. Advective forces are more dominant relative to density (i.e., buoyancy) forces with higher values of *MCR*. Abarca et al. (2007) found that penetration of the steady-state saltwater wedge toe decreases with increasing *MCR*, which infers strengthening advective forces (acting towards the sea) relative to the buoyancy force (in the inland direction).

Both mixed-convective and advective-dispersive processes differ between passive and active transient SWI situations. For example, density forces oppose advective forces in passive SWI, whereas in active SWI, density and advective forces act in the same direction. In the context of modelling a coastal cross section, this is invoked by freshwater outflow at the inland boundary under active SWI conditions and inflow for passive SWI conditions. It follows that the ratio of advective to buoyancy forces (i.e., *MCR*) is unlikely to be a feasible quantity for characterising the active SWI toe penetration extent, i.e., in the same manner that it is used in steady-state analyses (e.g., Abarca et al., 2007). However, other features of active SWI may respond to the balance of advective and buoyancy forces, and therefore, *MCR* may yet provide some useful application to the characterisation of active SWI.

The steady-state definition of *Pe* is (Abarca et al., 2004):

$$Pe = \frac{D_m n + \alpha_g q_f}{Q_f} \tag{3}$$

where α_g [L] is the geometric mean of dispersivity, i.e., $\sqrt{\alpha_T \alpha_L}$. Dispersion is more dominant relative to advection with higher values of *Pe*. This is invoked by wider mixing zones, but also the seawater penetration (at least at the toe) is shorter, for higher *Pe* values where the saltwater wedge is at steady state (Abarca et al., 2004). Under active SWI, both buoyancy and advective forces drive seawater advance, with the relative contributions of each likely to be reflected in *MCR* (although this is yet untested for active SWI problems). Thus, the form of *Pe* given in equation (3) is unlikely to inform active SWI behaviour in the same way that Abarca et al. (2004, 2007) found application of *Pe* to steady-state SWI. We examine this hypothesis in the main body of this article. An alternative to *Pe* for classifying active SWI problems is proposed and evaluated, involving the ratio of dispersion to the summation of buoyancy and advection. This accounts for the co-directional nature of buoyancy and advection, as:

$$A_{SWI} = \frac{D_m n + \alpha_g q_f}{Q_f + K\delta h_f} \tag{4}$$

Given similarities between steady-state and passive SWI (e.g., Morgan et al., 2012), *MCR* and *Pe*, defined respectively by equations (2) and (3), are expected to provide insights into passive SWI, if passive SWI is considered simple transitions from one steady-state condition to another. However, whether or not the same dimensionless parameters assist in characterising active SWI is unknown. For completeness, we compare Abarca et al.'s (2004; 2007) dimensionless parameters and A_{SWI} to both passive and active SWI to evaluate whether these offer some indication of transient SWI behaviour. This is the first attempt to link *MCR* and *Pe* to the characteristics of transient SWI.

We adopt $|q_f|$ and $|Q_f|$ for q_f and Q_f in discussing *Pe*, *MCR* and A_{SWI} in the remainder of the article to avoid negative values of these. Obviously, where steady conditions occur (i.e., after the cessation of passive SWI), Q_f equals Q_0. Preliminary model testing showed that in active SWI scenarios, q_f is largely stable once the abrupt hydraulic effects of the FHD have dissipated, and prior to the invasion of seawater at the inland boundary. Under these conditions, the rates of both seawater and freshwater flow (Q_s and Q_f, respectively) towards the inland boundary are equal. We considered this period of temporary flow constancy in applying non-dimensional parameters to active SWI. That is, q_f was obtained 15 y after the inland FHD in applying the above equations to active SWI. A check after 15 y showed that the mixing zone had not reached the inland boundary in all of the SWI cases, and Q_s and Q_f were effectively the same.

2.4. SWI response time-scales

Previously, Watson et al. (2010) and Lu and Werner (2013) measured SWI response time-scales by considering the final steady state as the terminal condition of passive SWI events. An alternative approach is required for active SWI cases given the lack of a steady-state condition, as discussed earlier. SWI response time-scales (T_i [T]) are defined in this article as the time for the 5%, 50% and 95% relative salinity contours at the aquifer base to reach a somewhat arbitrary inland location (termed here as x_{tb} [L]), measured from the sea boundary. x_{tb} was set to 95% of the distance between the original and post-FHD steady-state interface locations from the passive SWI base case (Case 1), with the 5% relative salinity contour representing the interface location. This is somewhat comparable to the Watson et al. (2010) and Lu and Werner (2013) approaches. Figure 2 shows the use of x_{tb} to determine T_i for the 5% relative salinity contour in the passive and active SWI base cases. For the passive SWI base case, x_{tb} is 386 m from the sea boundary and the corresponding T_i is 50.4 y. The same value of x_{tb} subsequently defines the values of T_i in all other SWI cases by obtaining the time required for the 5%, 50% and 95% relative salinity contours to move along the aquifer base to the position x_{tb}. For example, the value of T_i for the 5% relative salinity contour in the active SWI base case is 6.6 y (see Figure 2).

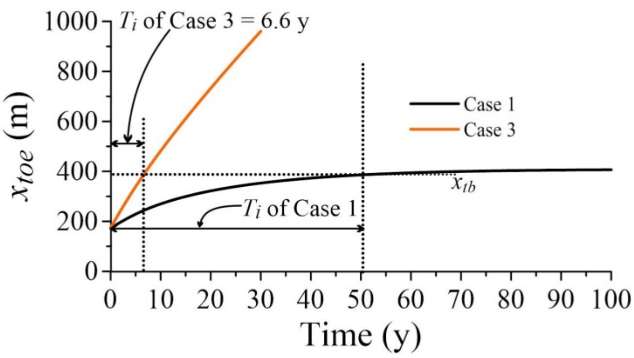

Figure 2. Estimation of T_i for the 5% relative salinity contour in the passive SWI (Case 1) and active SWI (Case 3) base cases.

3. Results and discussion

3.1. SWI sensitivity to parameter changes

3.1.1. Base cases of passive and active SWI

Figure 3 shows the transient interface movement of the passive and active SWI base cases. Following an instantaneous inland FHD, the interface advanced inland faster in the active SWI case relative to the passive SWI case, as expected. The mixing zone was wider under active SWI, and active SWI led to major salinization of the watertable, which was minor in the passive SWI case. Badaruddin et al. (2015) also reported these characteristics of active SWI. There was no outflow face (O_f) in both the active and passive SWI base cases, because the 5% relative salinity reached the watertable at the shoreline in the initial steady-state condition due to dispersive processes causing brackish groundwater discharge to the sea.

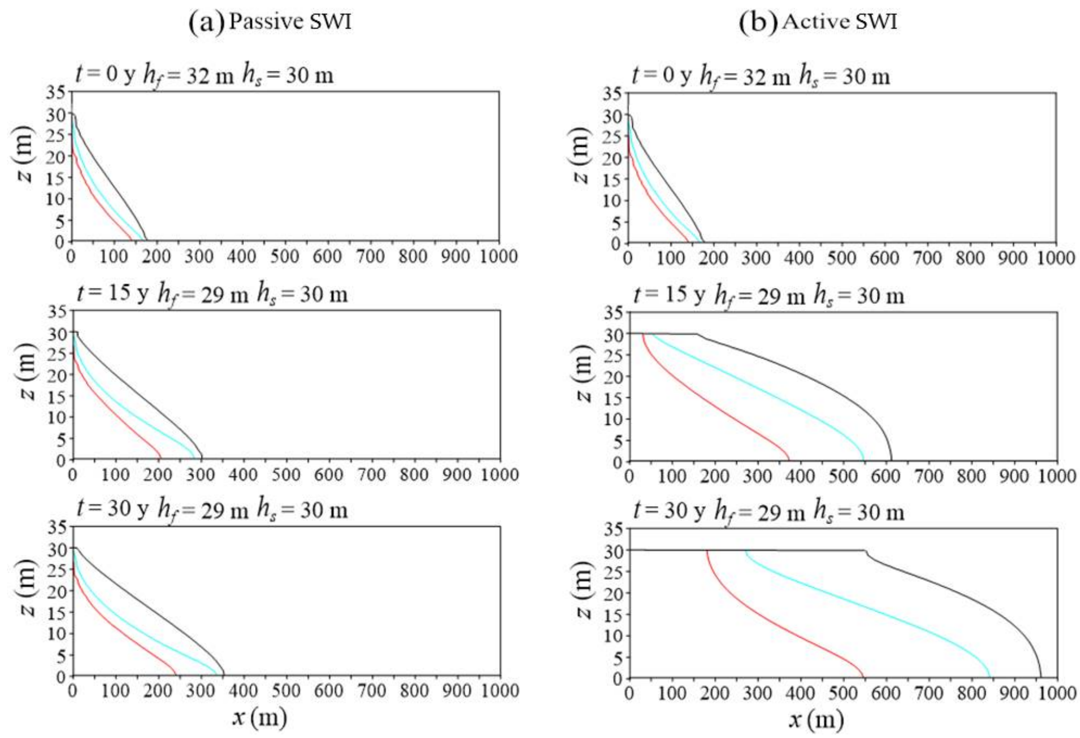

Figure 3. Distribution of the 5% (black line), 50% (blue line) and 95% (red line) relative salinity contours at 0 y, 15 y and 30 y for: (a) passive SWI base case (Case 1), and (b) active SWI base case (Case 3).

Figure 4 shows the temporal behaviour of key SWI measurables for the passive and active SWI base cases. Only the first 30 y are shown because simple continuations of trends were observed beyond that time (e.g., up to 100 y in the passive SWI base case).

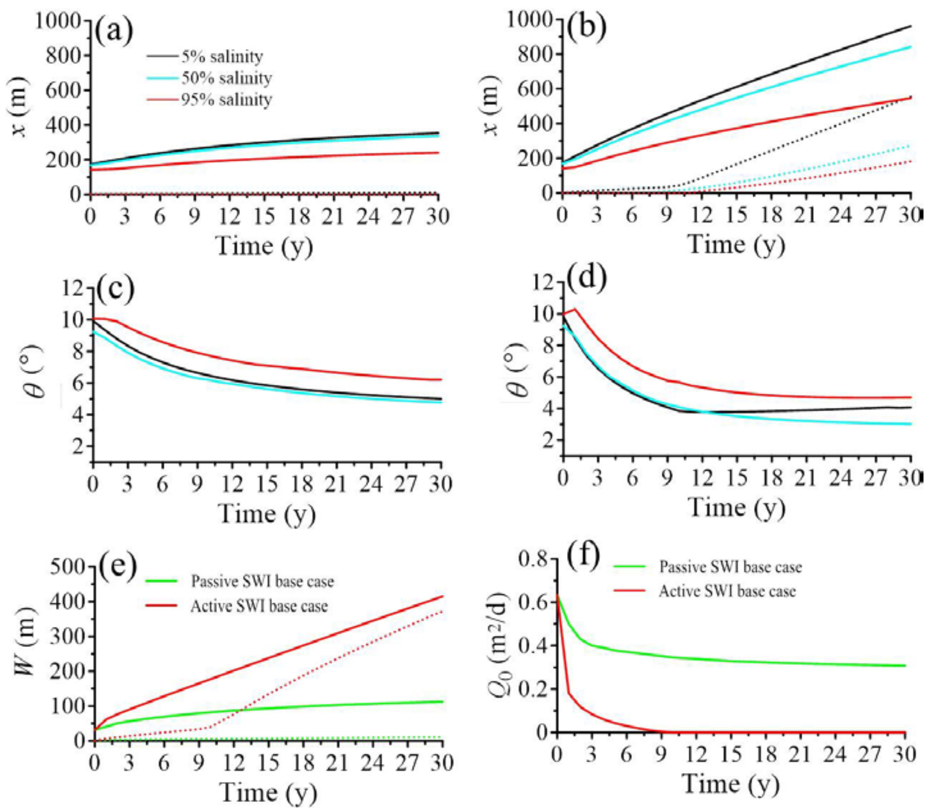

Figure 4. Transient changes in SWI measurables. (a) Case 1 toe and tip position, (b) Case 3 toe and tip position, (c) Case 1 interface slope, (d) Case 3 interface slope, (e) Cases 1 and 3 mixing zone widths, and (f) Cases 1 and 3 freshwater discharge to the sea. In (a), (b) and (e), solid and dotted lines are the interface toe and tip, respectively. The black, blue and red lines in (a) to (d) are the 5%, 50% and 95% relative salinities.

In the passive SWI base case, the toe (i.e., defined using three alternative salinities: 5%, 50% and 95%) moved inland gradually (Figure 4a), ceasing to advance after about 95 y. The tip effectively remained at the shoreline, although the 5% relative salinity contour stabilized at 18.0 m from the sea boundary (i.e., at the watertable). In contrast, the toe (e.g., in terms of the 5% relative salinity contour) almost reached the inland boundary (i.e., x = 961 m) after 30 y in the active SWI base case (Figure 4b). The tip (in terms of the 5% relative salinity contour) increased only slightly during the first 10 y of the active SWI case. Subsequently, the tip accelerated and maintained a higher inland velocity. Badaruddin et al. (2015) reported that this phenomenon is caused by the lag in the reduction of Q_0 to zero (and the accompanying reduction of O_f to zero), following the instantaneous FHD at the inland boundary. This is apparent in Figure 4f, which shows that in the active SWI base case, Q_0 dropped from the initial value of 0.63 m^2/d to 0 m^2/d after about 10 y, which coincides with the tip's acceleration (Figure 4b). In the passive SWI base case, Q_0 decreased and stabilised at 0.29 m^2/d.

In Figure 4c, θ in the passive SWI base case decreased throughout the first 30 y of the simulation for all three relative salinity contours. This reflects the lack of inland movement in the interface tip. In the active SWI base case, more complex trends in θ are apparent (Figure 4d). For the 5% relative salinity contour, θ decreased for the first 10 y and then increased thereafter. This shows that the interface tip velocity exceeded the interface toe velocity for times greater than 10 y, at least in terms of the 5% relative salinity contour. For the 50% relative salinity contour, θ decreased for the entire 30 y simulation period, while θ for the 95% relative salinity contour increased only in the early period of the simulation (i.e., 1 y after FHD). This occurred because of the rapid upward movement of the 95% relative salinity contour that accompanied the closure of the outflow face at the sea boundary.

Transient changes in the interface width (Figure 4e) show gradual widening, approaching asymptotic values of W_{toe} and W_{tip}, in the passive SWI base case. Lu et al. (2009) attributed interface widening under passive SWI to increases in flow velocities accompanying sea-level rise or an inland FHD. Interface widths at the tip and toe increased more rapidly in the active SWI base case, relative to the passive SWI base case, with W_{toe} following an almost linear trend after the cessation of Q_0, in a similar fashion to W_{tip}.

3.1.2. Effects of boundary head difference on active SWI

Figure 5 shows transient interface behaviour during the first 30 y of three active SWI simulations, in which different advective forcings were created by imposing alternative values of $h'_{f\text{-}s}$. That is, $h'_{f\text{-}s}$ is 0 m (Δh_f = 2 m), -1 m (Δh_f = 3 m; base case) and -2 m (Δh_f = 4 m) in Cases 2, 3 and 4, respectively. For $h'_{f\text{-}s}$ of -2 m, only the results for the first 20 y are shown because the 5% relative salinity contour reached the inland boundary around that time. Figure 5a shows that the tip and toe moved inland monotonically for all three $h'_{f\text{-}s}$ cases, approaching linearity at later times, although no significant movement of the interface tip was observed for the smallest head drop (Case 2). The decreasing trend in θ for the 50% relative salinity contour for all $h'_{f\text{-}s}$ variants (Figure 5b) indicates that the interface toe moved faster than the interface tip throughout the simulations. θ appears to tend towards asymptotic values with time that are higher (i.e., θ is steeper) for larger values of boundary head difference. That is, the landward advance of the interface tip eventually keeps pace with intrusion of the toe, and this occurs sooner with larger FHDs.

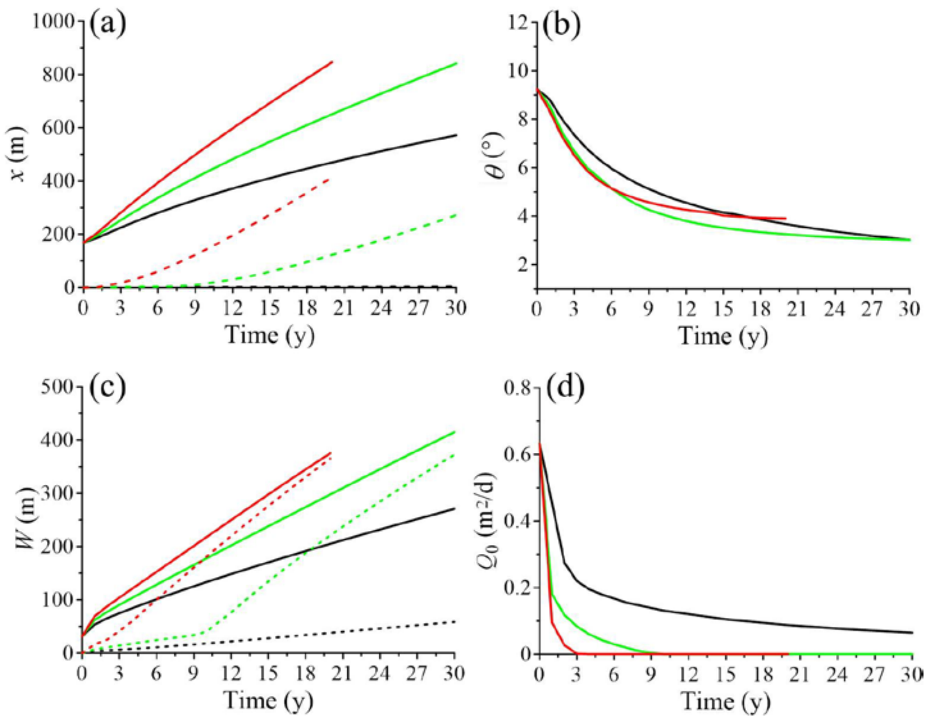

Figure 5. Effects of different final boundary head differences ($h'_{f\text{-}s}$ of 0 m (black; Case 2), -1 m (green; Case 3) and -2 m (red; Case 4)) on active SWI: (a) tip and toe, (b) slope based on the 50% relative salinity contour, (c) interface width, and (d) seaward freshwater discharge. Solid and dashed lines in (a) and (c) are the interface toe and tip, respectively.

Figure 5c shows that larger FHDs lead to more enhanced widening of the mixing zone with time. This effect is more pronounced for W_{tip} compared to W_{toe}. That is, W_{tip} increases are subtle (at least initially) where $h'_{f\text{-}s}$ is 0 m and -1 m, whereas a steep W_{tip} trend is obtained for $h'_{f\text{-}s}$ equal to -2 m. Inflexion in the W_{tip} trends for $h'_{f\text{-}s}$ -1 and -2 m occurred at 10 and 3 y, respectively, coinciding with closure of the outflow face and the cessation of Q_0 (Figure 5d). The largest FHD (Case 4) creates similar interface widening at the tip and toe.

3.1.3. Effects of *K*, *n*, α_L and h_s on active SWI

The effects of varying *K* (5, 10 and 20 m/d) and *n* (0.25, 0.30 and 0.35) on active SWI behaviour are presented in Figures 6a and 6b, respectively.

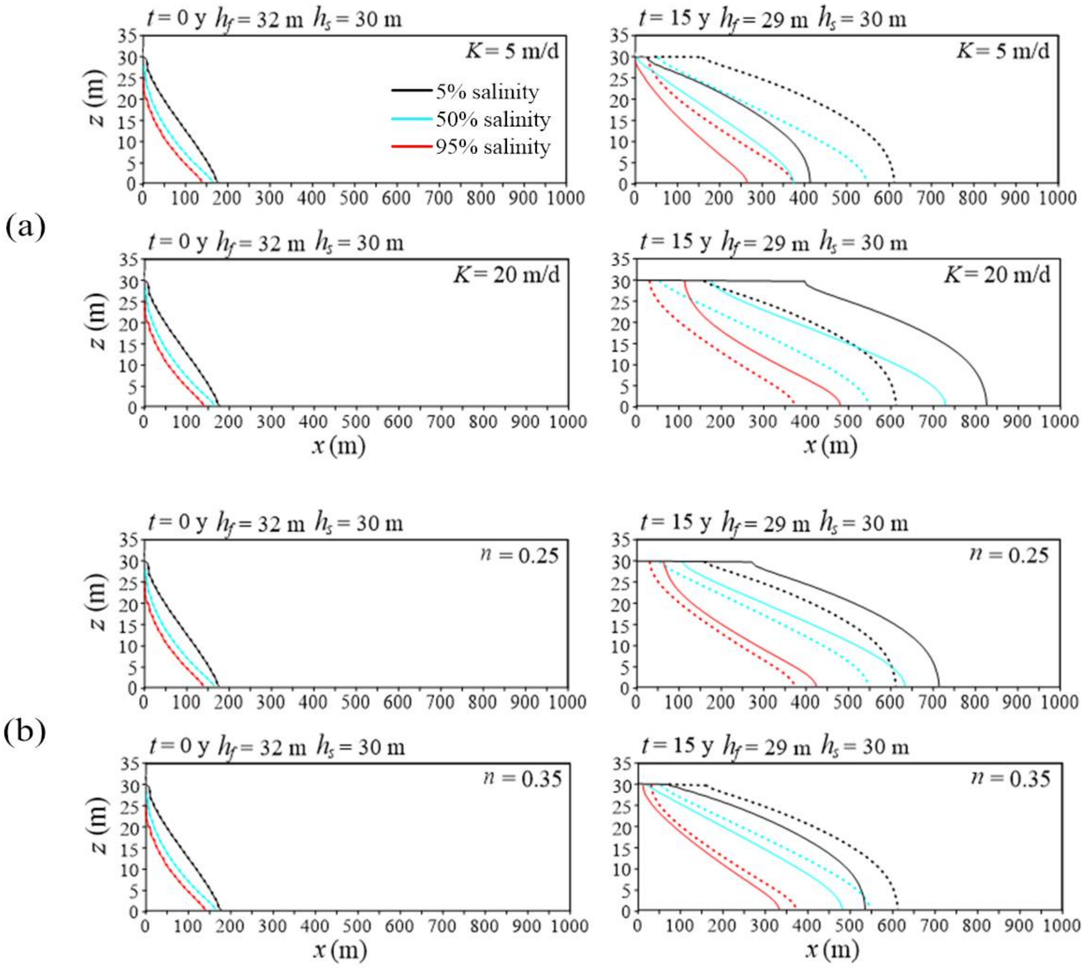

Figure 6. Distribution of the 5%, 50% and 95% relative salinity contours (solid lines) at 0 and 15 y using various values of: (a) hydraulic conductivity (Cases 7 and 11) and (b) porosity (Cases 39 and 43). Dashed lines represent salinity distributions of the active SWI base case.

Figure 6 shows that the initial steady-state salinity distribution was virtually unmodified by changes to *K* and/or *n*. This is justified below (Section 3.3) using *Pe* and *MCR*. The interface toe and tip moved faster and the mixing zone was wider with higher *K* and lower *n*, both of which create higher flow velocities. These active SWI observations are consistent with the passive SWI results of Lu and Werner (2013). They found that the change in the interface toe position (from one steady-state condition to another) is independent of the value of *K* and *n*, but that larger values of *K* or lower values of *n* lead to shorter interface toe response time-scales (i.e., faster interface movements). Figure 6 also shows that both higher *K* and lower *n* produced more WTS, resulting in steeper interface angles.

Figure 7 illustrates the effect of modifying (i.e., relative to Case 3) α_L and aquifer thickness on active SWI. Higher α_L led to rates of interface movement that were lower at the toe but higher at the tip (thereby increasing θ), and resulted in mixing zone widths that were larger both at the toe and tip (Figure 7a). This is consistent with the steady-state SWI findings of Kerrou and Renard (2010), who found that stronger dispersion leads to decreased density contrasts due to the wider mixing zone. This condition causes rotation of the mixing zone alignment such that the interface toe moves seaward relative to the interface tip. Figure 7b shows that under transient conditions, the rates of both toe and tip movement were higher for thicker aquifers. This is in accordance with Badaruddin et al. (2015), who showed that under active SWI conditions, the toe and tip move faster inland in thicker aquifers, for a given $h'_{f\text{-}s}$. The interface slope was slightly shallower for thicker aquifers. This is attributable to the stronger buoyancy effect in deeper aquifers (e.g., the equivalent freshwater head increases with depth at the sea boundary) that drives landward rotation of the interface toe relative to the interface tip.

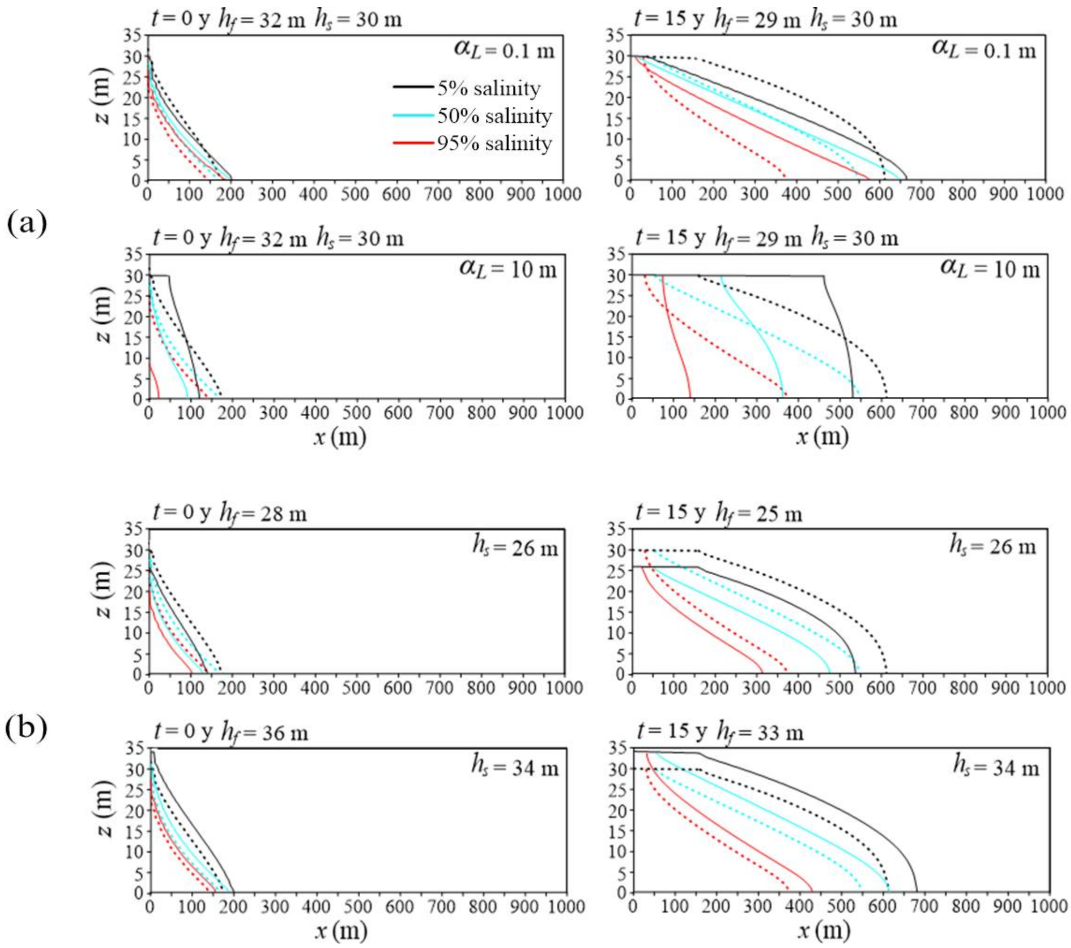

Figure 7. Distribution of the 5%, 50% and 95% relative salinity contours at 0 and 15 y using various values of: (a) longitudinal dispersivity (Cases 15 and 19) and (b) aquifer thickness (Cases 31 and 35). Dashed lines represent salinity distributions of the active SWI base case.

3.1.4. Effects of buoyancy on active SWI

The influences of modifying seawater density relative to the active SWI base case are shown in Figure 8. As expected, the interface toe and tip moved faster with higher ρ_s, and the stronger buoyancy force produced a shallower interface slope. Higher ρ_s also resulted in wider mixing zones. This adds to previous observations of density effects on SWI, although Schincariol (1998) noticed increased mixing with larger density contrasts in free convection problems.

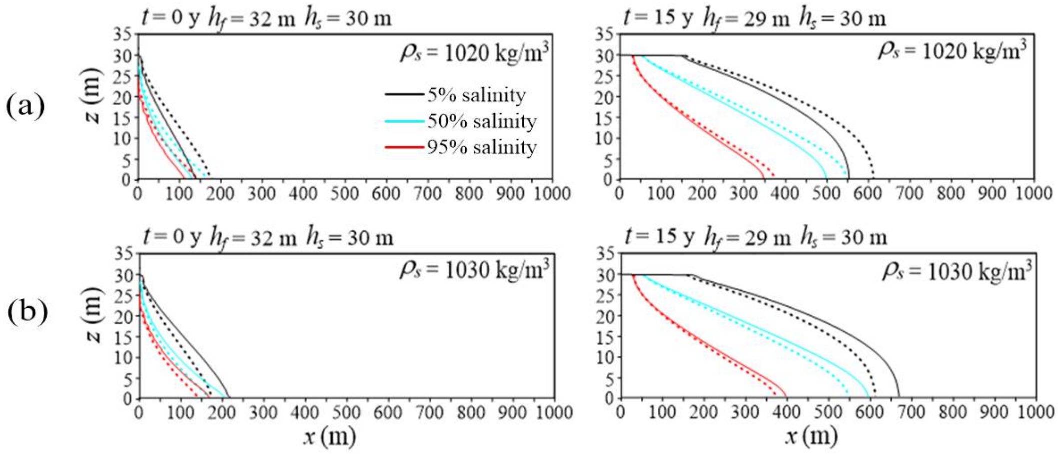

Figure 8. Distribution of the 5%, 50% and 95% relative salinity contours at 0 and 15 y using various values of seawater density: (a) 1020 kg/m^3 (Case 23), and (b) 1030 kg/m^3 (Case 27). Dashed lines represent salinity distributions of the active SWI base case.

Under the initial steady-state conditions illustrated in Figure 8, increasing ρ_s from 1020 kg/m^3 to 1030 kg/m^3 lowered q_f from 0.017 m/d to 0.015 m/d. The active SWI results showed contrasting ρ_s effects on q_f, which increased with higher ρ_s (i.e., after 15 y of active SWI, q_f was 0.013 m/d and 0.015 m/d in Cases 23 and 27, respectively). Higher ρ_s led to wider mixing zones in both steady-state and active SWI modes. That is, in Cases 23 and 27, W_{toe} was initially 21.4 and 44.5 m, respectively, and after 15 y of active SWI, these values increased to 205 and 271 m, respectively.

The evaluation of buoyancy effects was extended by comparing advective velocities $(v = q_f / n)$ to the velocities of the toe and tip at 15 years after the FHD for all 1 km-scale active SWI cases in Table 1. The same analysis is not possible for passive SWI cases, because there is no corresponding period of stable toe velocity. The 50% salinity contour was used to represent the toe and tip. The interface positions at 15.08 y and 15.16 y for both the toe and the tip were adopted in calculating their respective velocities. The temporal toe and tip trends were near-linear at this time (see Figure 5a) and hence we adopt these as representative toe and tip velocities for each case. We presume that differences between the interface velocities of active SWI and the advective transport rate (*v* [L/T]) are an indication of the effect of density on active SWI. The results are presented in Figure 9, which shows the velocity differences (interface velocity minus *v*) of active SWI cases (i.e. $h'_{f\text{-}s}$ equal to 0, -1 and -2 m).

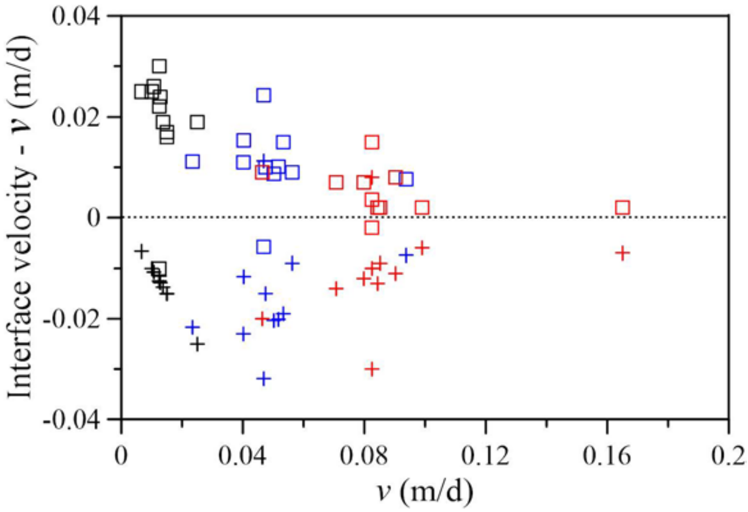

Figure 9. Scatter plot of the differences between the groundwater velocity (*v*) and the interface toe (□) and tip (+) in active SWI simulations. Black, blue and red symbols represent the cases with $h'_{f\text{-}s}$ of 0, -1 and -2 m, respectively.

Figure 9 shows that differences between active interface velocities and *v* become smaller as SWI becomes more active (i.e., as the interface velocity increases), highlighting the relatively stronger effect of advection. In general, the tip moves slower and the toe moves faster than *v*. The toe velocity is closer to *v* than the tip velocity, indicating that the tip velocity is more responsive to density effects. The relative effect of buoyancy on velocities is quantified using |1 – interface velocity/*v*|, which falls to less than 0.10 (< 10% buoyancy effect on velocities) for *v* > 0.08 m/d. For these cases, we argue that the rate of active SWI can be reasonably estimated using density-independent formulae.

3.2. Active SWI response time-scales

In this section, we compare time-scales of active SWI to those of passive SWI reported by Lu and Werner (2013), who observed a linear relationship between the response time-scale T_i and the exponential of the final boundary head differences $(e^{h'_{f-s}})$. Figure 10 shows T_i for 5%, 50% and 95% relative salinity contours versus $e^{h'_{f-s}}$. Several different values of Δh_f were used (i.e., Δh_f ranging from 2 to 4 m; Cases 2 to 4 and 45 to 64) to create multiple series of T_i versus $e^{h'_{f-s}}$. The two variables were related using a simple linear relationship similar to the approach of Lu and Werner (2013), as:

$$T_i = a + be^{h'_{f-s}} \quad (5)$$

Here, a and b are coefficients obtained by linear regression. Their values differed depending on Δh_f. A strong correlation was observed in the linear regression between T_i and $e^{h'_{f-s}}$ values, as indicated by values of the determination coefficient R^2 [-], which ranged from 0.97 to 0.99 (the values of a, b, and R^2 resulted from a larger modelling dataset than the subset used to produce Figure 10 are provided in Appendix A).

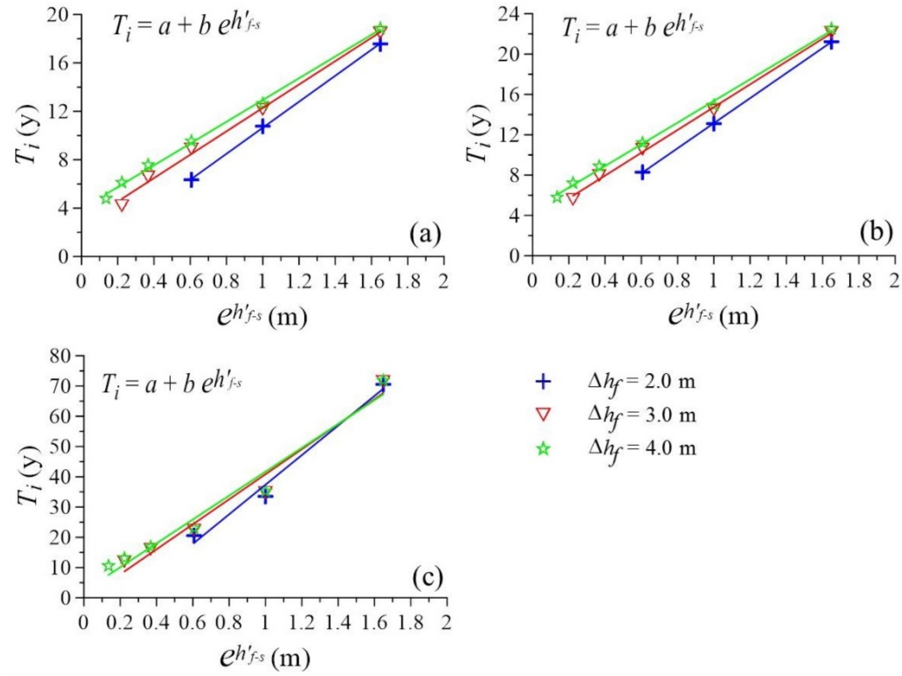

Figure 10. Linear regressions between $e^{h'_{f-s}}$ and T_i for: (a) the 5% relative salinity contour, (b) the 50% relative salinity contour, and (c) the 95% relative salinity contour, based on Cases 2 to 4 and 45 to 64.

The current analysis of time-scales differs to the approach of Lu and Werner (2013) in that the final interface location for defining T_i in the current study (i.e., x_{tb} = 386 m from the sea boundary) was the same in all cases, as discussed above. Figure 10 shows that for equal values of Δh_f, T_i values increased with less steep head gradients in the inland direction (i.e., $h'_{f\text{-}s}$ becomes more positive). In other words, SWI slows down and the time-scale increases as the inland head gradient becomes shallower, as expected. This is in accordance with the passive SWI results of Lu and Werner (2013). Figure 10 also shows that for a given $h'_{f\text{-}s}$, T_i increases with larger Δh_f, more noticeably for the 5% and 50% relative salinities. Longer time-scales occur with larger Δh_f because the interface has further to travel, given that the initial interface is closer to the coast with increasing Δh_f. This indicates that besides the final boundary head difference, the initial boundary head difference also influences active SWI time-scales, unlike

Lu and Werner's (2013) observation of passive SWI, in which only $h'_{f\text{-}s}$ modifies T_i. This outcome is at least partly attributable to the manner in which T_i has been obtained in the two studies, whereby Lu and Werner (2013) recalculated x_{tb} for each case, rather than the fixed value adopted in the current analysis, as described above. Nevertheless, the key outcome of this analysis is that active SWI time-scales are linearly related to $e^{h'_{f-s}}$, consistent with the passive SWI findings of Lu and Werner (2013), despite that our definition of T_i is unavoidably modified relative to that used by Lu and Werner (2013).

3.3. *MCR*, *Pe* and A_{SWI} as indicators of passive and active SWI characteristics

In this section, dimensionless parameters are evaluated in terms of their ability to predict various characteristics of steady-state interface conditions and active SWI. Steady-state conditions were adopted as a surrogate for passive SWI in testing dimensionless parameters for reasons given in Section 2.3. Firstly, we reviewed the direction of sensitivities between SWI variables and model parameters, as given in Table 2. The complete results of SWI variables for the passive and active SWI cases listed in Table 1 are provided in Appendix B and C, respectively.

Table 2. Trends in SWI variables as a function of increases in the values of model parameters, arising from the sensitivity analysis.

SWI variable	Model parameters					
	K	α_L	ρ_S	h_s	n	$\lvert h'_{f\text{-}s}\rvert$
Passive SWI						
x_{toe} (50% contour)	None	Falling	Rising	Rising	None	Falling
W_{toe}	None	Rising	Rising	Rising	None	Falling
θ (50% contour)	None	Rising	Falling	Falling	None	Rising
Active SWI						
x_{toe} (50% contour)	Rising	Falling	Rising	Rising	Falling	Rising
x_{tip} (50% contour)	Rising	Rising	Rising*	Rising	Falling	Rising
W_{toe}	Rising	Rising	Rising	Rising	Falling	Rising
W_{tip}	Rising	Rising	Rising	Rising	Falling	Rising
θ (50% contour)	Falling*	Rising	Falling	Falling*	Rising*	Mixed

"None" means that the SWI variable is insensitive to the parameter
"Rising" means that the SWI variable increases with an increase in parameter value
"Falling" means that the SWI variable decreases with an increase in parameter value
"Mixed" means that there is no predominant trend.
"*" refers to variables where a predominant trend is noted, but exceptions apply.

Table 2 highlights complex relationships between SWI variables and model parameters, whereby none of the SWI variables show the same type of response (i.e. rising, falling, etc.) to parameter changes under both passive and active SWI conditions. Under steady-state conditions, x_{toe} (50% contour) and θ (50% contour) respond in an opposing manner because of the general immobility of x_{tip}. Under transient (i.e., active SWI) conditions, x_{tip} (50% contour), W_{toe} and W_{tip} respond in the same general fashion, but differently to θ (50% contour) and x_{toe} (50% contour).

Some of the SWI responses are predictable using *Pe* and *MCR*. For example, the initial steady-state salinity distribution of the base case model was virtually unmodified by changes to K and/or n (see Section 3.1.3). These insensitivities are recorded in Table 2 as "None", and can be justified by considering *Pe* and *MCR* for steady-state conditions. That is, *Pe* is dominated by α_g/h_f given that D_m is small, and therefore *Pe* is largely independent of both K and n (see equation (3)). In equation (2), q_f/K is approximately proportional to $h'_{f\text{-}s}$ under steady-state conditions due to the specified-head boundaries, and therefore *MCR* is also essentially independent of *K* and *n*. However, both *K* and *n* play an important role in active SWI, as illustrated in Figure 6 and identified in Table 2. This highlights important differences between the controlling factors of active and steady-state SWI.

Drawing on equations (2) to (4), some of the responses in SWI variables to parameter changes can be linked to dimensionless parameters. For example, steady-state x_{toe} (50% salinity contour) increases with lower α_L and $h'_{f\text{-}s}$, and with higher ρ_s and h_f. The effects of ρ_s and $h'_{f\text{-}s}$ are captured within the definition of *MCR* (equation (2)), whereas the effects of α_L and h_f are contained within *Pe* and A_{SWI} (equations (3) and (4)). Linear correlation between steady-state x_{toe} (50% salinity contour) and *MCR* results in a falling trend and R^2 = 0.77, indicating the dominant influences of ρ_s and $h'_{f\text{-}s}$ in controlling steady-state x_{toe}. Efforts to correlate steady-state x_{toe} with *Pe* were unsuccessful ($R^2 < 0.14$), and therefore α_L and h_f are minor factors relative to ρ_s and $h'_{f\text{-}s}$ in controlling x_{toe} for the steady-state cases considered here.

MCR showed similar correlation statistics when linearly related to the transient x_{toe} and x_{tip} positions, producing R^2 values of 0.61 and 0.71, respectively. While steady-state x_{toe} generally reduces with increasing *MCR*, transient x_{toe} and x_{tip} tend to be larger with higher *MCR*. It is important to note that relatively few unique values of δ have been tested in obtaining these relationships (see Table 1). Thus, the active SWI results reflect x_{toe} and x_{tip} that are further inland with stronger discharge (q_f; in the landward direction), rather than mixed convection processes. Hence, we maintain that *MCR* is a poor indicator of active SWI behaviour, in terms of the effects of mixed-convective processes on x_{toe} and x_{tip}. However, *MCR* has a more logical association with the interface slope, given Kerrou and Renard's (2010) observations, as mentioned earlier, and indeed, *MCR* shows some correlation with steady-state θ (50% contour), with $R^2 = 0.65$. No significant correlation was apparent between MCR and active SWI θ (50% contour). Rather, both steady-state and active SWI θ (50% contour) show some correlation to A_{SWI}, with R^2 values of 0.61 and 0.80, respectively. A weaker correlation between Pe and steady-state and active SWI θ was obtained (R^2 equal to 0.30 and 0.49, respectively). These results highlight the complex mixed convective and convective-dispersive relationships that govern interface slope under transient SWI conditions.

Surprisingly, Pe was found to be a poor indicator of steady-state W_{toe}, with R^2 of 0.11. In fact, MCR outperformed Pe in terms of its linear correlation with steady-state W_{toe}, producing R^2 = 0.67. This is in contradiction to the findings of Abarca et al. (2004). In active SWI cases, Pe was similarly a poor predictor ($R^2 < 0.26$) of W_{toe} and W_{tip}. A_{SWI} also produced a weak match to active SWI W_{toe} and W_{tip} (R^2 of 0.42 and 0.44, respectively), albeit slightly improved relative to Pe.

No correlation was found between Pe and steady-state x_{toe} or active SWI x_{toe} and x_{tip} ($R^2 <$ 0.12), despite Abarca et al. (2004) suggesting smaller toe penetration with higher Pe. A_{SWI} was similarly poorly performing as a measure of interface location in active SWI cases ($R^2 < 0.30$), although R^2 for A_{SWI} versus steady-state x_{toe} was 0.56 using a power function.

The results suggest that the dimensionless forms of Pe and MCR used in the current study cannot be used to generalise without exception the sensitivity and response of the freshwater-saltwater interface to changes in various aquifer parameters. Nonetheless, the dimensionless numbers remain useful indicators of buoyancy, advective and dispersive controls, which influence the interface behaviour in predictable ways under certain conditions, as described above. Despite the inability of the dimensionless numbers tested here to consistently predict interface changes arising within the one-at-a-time sensitivity analysis carried out in this study, both under steady-state and active SWI conditions, we have been unable to define new dimensionless variables with improved performance in characterising active SWI.

3.4. Field-scale example of SWI

A field-scale SWI example is included here to extent the 1 km-scale analysis described above, and to test whether previous sensitivities have application that is more general. As stated previously, Case 65 represents a field-scale SWI case, with parameters typical of those found in the Pioneer Valley aquifer, Australia (Werner and Gallagher, 2006). The relevant parameters are listed in Table 1, and the transient interface behaviour for this case is presented in Figure 11, which shows aggressive inland movement of the interface toe and tip, following the inland FHD. At the initial steady-state, the values of *Pe* and *MCR* in this case are 0.076 and 0.030, respectively. At 15 y after the FHD, *Pe* and *MCR* increased to 0.087 and 0.037, respectively. These values of *Pe* and *MCR* are best matched, in terms of 1 km-scale active SWI cases, to those of Case 19 (i.e. *Pe* = 0.11; *MCR* = 0.056). Nevertheless, the magnitudes of W_{toe} and W_{tip} (after 15 y) for Case 65 are approximately five times larger than those in Case 19 (see Appendix C). This is likely due to the higher *K* (166 m/d) and lower *n* (0.1) values (in Case 65), which increase the flow velocity in this case (q_f = 0.15 m/d) relative to Case 19 (q_f = 0.014 m/d).

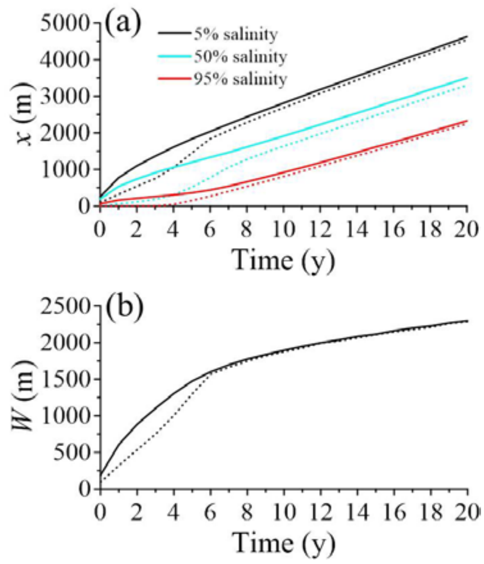

Figure 11. Transient changes of: (a) interface locations and (b) interface width, for Case 65. Solid and dotted lines represent the interface toe and tip, respectively.

To examine the effects of aquifer parameters on the interface position and width in the field-scale case, sensitivity analyses were conducted with increasing K (332 m/d), α_L (20 m), ρ_s (1030 kg/m^3), h_s (40 m) and n (0.2), using Case 65 as the base case (the results are not shown for brevity). It was observed that for a given $h'_{f\text{-}s}$, the x_{toe} increased with increasing K, ρ_s and h_s and decreased with increasing α_L and n. In addition, the x_{tip} and the mixing zone width (at the toe and tip) increased with increasing K, ρ_s, h_s and α_L and decreased with increasing n. These trends are consistent with those found for the cases adopting smaller domain sizes (Table 2).

To explore the relationship between SWI response time-scales and the inland FHD in the field-scale case, more SWI simulations were undertaken using five different values of $h'_{f\text{-}s}$ (from -0.4 to -2 m, in increments of 0.4 m), using Case 65 as the base case. Five values of Δh_f were adopted for each $h'_{f\text{-}s}$ value (i.e., 5.4, 5.8, 6.2, 6.6 and 7 m), resulting in 25 more SWI simulations. The arbitrary point of x_{tb} used for the field-scale cases was 1133 m (obtained from the 95% of the distance between the original and post-FHD steady-state interface locations of the 5% relative salinity in the passive SWI field case with $h'_{f\text{-}s}$ = 1 m) from the sea boundary. It was observed that the final and the initial boundary head differences influence the SWI time-scales in the field-scale cases (Figure 12). The SWI response time-scales are also linearly related to $e^{h'_{f-s}}$, as indicated by high values of R^2 that ranged from 0.98 to 0.99 (the values of a, b and R^2 resulted from a larger modelling dataset than that given in Figure 12 and are provided in Appendix D). These results are in accordance with the results of the non-field cases.

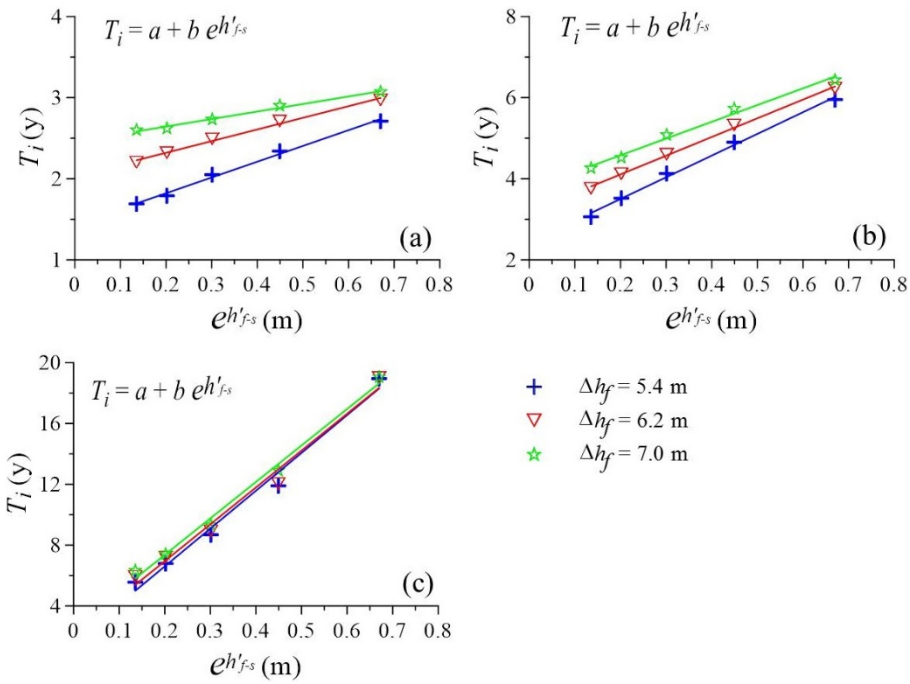

Figure 12. Linear regressions between $e^{h'_{f-s}}$ and T_i for: (a) the 5% relative salinity contour, (b) the 50% relative salinity contour, and (c) the 95% relative salinity contour, in the field-scale cases.

There are important features of field settings that the current analysis has neglected, but that may be important factors in real-world occurrences of active SWI. For example, sudden changes in boundary conditions, as adopted here, are rare. Even where groundwater declines are considerable, such as the Llobregat Delta aquifer (Vázquez-Suñé et al., 2006), the rate of water level fall usually occurs over several decades. Our sudden head drop creates immediate disequilibrium between the boundary conditions and the flow and salinity distributions, whereas disequilibrium may occur to less extreme degrees in field situations where active SWI is observed. Another practical limitation of the current analysis is that we truncate the aquifer at the shoreline, despite that in many cases, coastal aquifers continue offshore. It is likely that the active SWI processes shown in the current study hold some relevance to the freshwater bodies of offshore, confined and semi-confined aquifers, although further analysis is required to assess SWI under subsea conditions. Finally, the ubiquitous heterogeneity of coastal sediments has been neglected in our modelling experiments, whereas the spatial variability in aquifer properties no doubt plays an important role in the occurrence of active SWI in real-world systems.

4. Conclusions

The current study is the first attempt to characterize freshwater-saltwater interface characteristics during active SWI conditions. Aside from conforming to several of the active SWI observations of Badaruddin et al. (2015), our sensitive analysis reveals other important features of active SWI. For example, while the interface slope gradually became shallower during passive SWI, trends in the interface angle during active SWI simulations were complex. That is, active SWI can sometimes lead to interface tip movements that are faster than the interface toe velocity. The interface tip eventually kept pace with the toe, particularly for increasingly active SWI, which also led to widening of the mixing zone with time, especially at the interface tip. Furthermore, the interface toe and tip moved faster and the mixing zone was wider with higher K and lower n, both of which created higher flow velocities. These observations of active SWI match those by Lu and Werner (2013) for passive SWI. However, only in active SWI does higher K and lower n produce more watertable salinization, resulting in steeper interface angles. In addition, higher α_L led to rates of interface movement that were lower at the toe but higher at the tip (thereby increasing interface alignment), and resulted in mixing zone widths that were larger both at the toe and tip. This result overlaps with observations of steady-state SWI characteristics by Kerrou and Renard (2010). The interface slope was slightly shallower for thicker aquifers due to stronger buoyancy effects in deeper aquifers.

As expected, the interface toe and tip moved faster with higher seawater density, and the stronger buoyancy force produced a shallower interface slope. Higher seawater density also resulted in wider mixing zones. This adds to previous observations of density effects on SWI. Differences between interface velocities under active SWI and the advective transport rates were used as an indication of the effect of density on active SWI. The effect of advection was found to increase as SWI became more active. The toe velocity was closer to the advective transport rate than the tip velocity, indicating that the tip velocity was more responsive to density effects. It was found that the rate of active SWI could be reasonably estimated using density-independent formulae when the advective transport rate was greater than 0.08 m/d.

Based on the numerical modelling results, we conclude that active SWI time-scales are linearly related to $e^{h'_{f-s}}$, consistent with the passive SWI findings of Lu and Werner (2013), despite that our definition of T_i was unavoidably modified relative to that used by Lu and Werner (2013). A field-scale SWI example showed that the effects of aquifer parameters on interface behaviour and the time-scales showed consistent trends to the 1 km-scale models.

The transient nature of our active SWI investigation adds to the primarily steady-state assessment in a concurrent analysis by Werner (2017). For example, the link between mixing zone width and the freshwater-seawater density difference highlight critical differences between active SWI and slower rates of SWI. As a general concept, coastal aquifer custodians should consider SWI to increasing resemble density-independent plumes as the disequilibrium between the coastal head and inland heads increases. It follows that under intensive active SWI conditions (i.e., steep head gradients sloping towards the land), salinization is more likely to eliminate the freshwater normally found in the shallow part of the aquifer. The current results, combined with Werner's (2017) modelling show that this effect is particularly dependent on density and dispersive parameters, and the degree of disequilibrium. We also find that the cessation of discharge to the sea is the trigger for considerable losses of fresh groundwater in the upper aquifer, in some circumstances at rates that exceed the rate of the wedge toe movements. Thus, coastal aquifer custodians are encouraged to adopt management strategies that avoid the termination of freshwater discharge to the sea even where active SWI is occurring, to avoid this deleterious effect.

Our attempts to describe active SWI in terms of dimensionless parameters, which are widely used for steady-state SWI, were unsuccessful. Specifically, the results demonstrate that the dimensionless parameters of *Pe* and *MCR* were unable to consistently predict interface changes arising within the sensitivity analysis, at least in terms of consistency in both steady-state and active SWI conditions. Complex relationships were found to occur between SWI variables and model parameters, whereby none of the SWI variables show the same type of response (i.e., rising, falling, etc.) to parameter changes under both passive and active SWI conditions. This highlights important differences between the controlling factors of active and steady-state SWI.

Further work is needed to define new dimensionless variables with improved performance in characterising active SWI.

Acknowledgements

This research is a part of the PhD thesis of the first author at Flinders University. We thank the Australia Awards Scholarship for funding the first author's study at Flinders University. Adrian Werner is the recipient of an Australian Research Council Future Fellowship (project number FT150100403). We also gratefully acknowledge the suggestions of three anonymous reviewers and the guest editor (Vincent Post).

References

Abarca, E., J. Carrera, R. Held, X. Sanchez-Vila, M. Dentz, W. Kinzelbach and E. Vazquez-Sune (2004). Effective dispersion in seawater intrusion through heterogeneous aquifer. 18th Salt Water Intrusion Meeting, Cartagena, Spain, IGME, 31 May – 3 June 2004.

Abarca, E., Carrera, J., X. Sánchez-Vila and M. Dentz (2007). Anisotropic dispersive Henry problem. Advances in Water Resources 30: 913-926, doi: 10.1016/j.advwatres.2006.08.005.

Badaruddin, S., A. D. Werner and L. K. Morgan (2015). Watertable salinization due to seawater intrusion. Water Resources Research 51: 8397-8408, doi: 10.1002/2015WR017098.

Bear, J. (1979). Hydraulics of Groundwater. First ed. McGraw-Hill. New York. 569pp.

Bocanegra, E., G. C. Da Silva Jr, E. Custodio, M. Manzano and S. Montenegro (2010). State of knowledge of coastal aquifer management in South America. Hydrogeology Journal 18: 261-267, doi: 10.1007/s10040-009-0520-5.

Brovelli, A., X. Mao and D. A. Barry (2007). Numerical modeling of tidal influence on density-dependent contaminant transport. Water Resources Research 43: 1-15, doi: 10.1029/2006WR005173.

Chang, S. W., T. P. Clement, M. J. Simpson and K. K. Lee (2011). Does sea-level rise have an impact on saltwater intrusion? Advances in Water Resources 34: 1283-1291, doi: 10.1016/j.advwatres.2011.06.006.

Custodio, E. (2010). Coastal aquifers of Europe: an overview. Hydrogeology Journal 18: 269-280, doi: 10.1007/s10040-009-0496-1.

Fetter, C. W. (2001). Applied hydrogeology. Fourth ed. Prentice Hall Inc. New Jersey. 598pp.

Goswami, R. R. and T. P. Clement (2007). Laboratory-scale investigation of saltwater intrusion dynamics. Water Resources Research 43: 1-11, doi: 10.1029/2006WR005151.

Henry, H. R. (1964). Effects of dispersion on salt encroachment in coastal aquifers. Sea Water in Coastal Aquifers. US Geological Survey Water Supply Paper 1613 – C: 70-84.

Held, R., S. Attinger and W. Kinzelbach (2005). Homogenization and effective parameters for the Henry problem in heterogeneous formations. Water Resources Research 41: 1-14, doi: 10.1029/2004WR003674.

Kerrou, J. and P. Renard (2010). A numerical analysis of dimensionality and heterogeneity effects on advective dispersive seawater intrusion processes. Hydrogeology Journal 18: 55-72, doi: 10.1007/s10040-009-0533-0.

Langevin, C. D., W. B. Shoemaker and W. Guo (2003). MODFLOW-2000, the US Geological Survey Modular Ground-Water Model-Documentation of the SEAWAT-2000 Version with the Variable-Density Flow Process (VDF) and the Integrated MT3DMS Transport Process (IMT). USGS Department of the Interior. http://fl.water.usgs.gov/PDF_files/ofr03_426_langevin.pdf (accessed 13 April, 2016).

Langevin, C. D., D. T. Thorne Jr., A. M. Dausman, M. C. Sukop and W. Guo (2008). SEAWAT Version 4: a computer program for simulation of multi-species solute and heat transport (No. 6-A22). USGS Department of the Interior. http://pubs.usgs.gov/tm/tm6a22/pdf/tm6A22.pdf (accessed 13 April, 2016).

Lu, C., P. K. Kitanidis and J. Luo (2009). Effects of kinetic mass transfer and transient flow conditions on widening mixing zones in coastal aquifers. Water Resources Research 45: 1-17, doi: 10.1029/2008WR007643.

Lu, C. and A. D. Werner (2013). Timescales of seawater intrusion and retreat. Advances in Water Resources 59: 39-51, doi: 10.1016/j.advwatres.2013.05.005.

Mahesha, A. (1995). Parametric studies on the advancing interface in coastal aquifers due to linear variation of the freshwater level. Water Resources Research 31: 2437-2442, doi: 10.1029/95WR02040.

Morgan, L. K., A. D. Werner and C. T. Simmons (2012). On the interpretation of coastal aquifer water level trends and water balances: A precautionary note. Journal of Hydrology 470: 280-288, doi: 10.1016/j.jhydrol.2012.09.001.

Morgan, L. K., L. Stoeckl, A. D. Werner and V. E. A. Post (2013). An assessment of seawater intrusion overshoot using physical and numerical modelling. Water Resources Research 49: 6522-6526, doi: 10.1002/wrcr.20526.

Morgan, L. K. and A. D. Werner (2015). A national inventory of seawater intrusion vulnerability for Australia. Journal of Hydrology: Regional Studies 4, 686-698, doi; 10.1016/j.ejrh.2015.10.005.

Morgan, L. K., M. Bakker and A. D. Werner (2015). Occurrence of seawater intrusion overshoot. Water Resources Research 51: 1989-1999, doi: 10.1002/2014WR016329.

Schincariol, R. A. (1998). Dispersive mixing dynamics of dense miscible plumes: natural perturbation initiation by local-scale heterogeneities. Journal of Contaminant Hydrology 34: 247-271, doi: 10.1016/S0169-7722(98)00081-3.

Sebben, M. L., A. D. Werner and T. Graf (2015). Seawater intrusion in fractured coastal aquifers: A preliminary numerical investigation using a fractured Henry problem, Advances in Water Resources 85: 93-108, doi: 10.1016/j.advwatres.2015.09.013.

Simpson, M. J. and T. P. Clement (2003). Theoretical analysis of the worthiness of henry and elder problems as benchmarks of density-dependent groundwater flow models. Advances in Water Resources 26: 17-31, doi: 10.1016/S0309-1708(02)00085-4.

Vázquez-Suñé, E., E. Abarca, J. Carrera, B. Capino, D. Gámez, M. Pool, T. Simó, F. Batlle, J. M. Niñerola and X. Ibáñez (2006). Groundwater modelling as a tool for the European

Water Framework Directive (WFD) application: The Llobregat case. Physics and Chemistry of the Earth 31(17): 1015-1029, doi: 10.1016/j.pce.2006.07.008.

Voss, C. I. and W. R. Souza (1987). Variable density flow and solute transport simulation of regional aquifers containing a narrow freshwater-saltwater transition zone. Water Resources Research 23: 1851-1866, doi: 10.1029/WR023i010p01851.

Watson, T. A., A. D. Werner and C. T. Simmons (2010). Transience of seawater intrusion in response to sea-level rise. Water Resources Research 46: 1-10, doi: 10.1029/2010WR009564.

Webb, M. D. and K. W. Howard (2011). Modeling the transient response of saline intrusion to rising sea-levels. Ground Water 49: 560-569, doi: 10.1111/j.1745-6584.2010.00758.x.

Werner, A. D. (2017). On the classification of seawater intrusion. Journal of Hydrology, In press, doi: 10.1016/j.jhydrol.2016.12.012.

Werner, A. D. and D. A. Lockington (2006). Tidal impacts on riparian salinities near estuaries. Journal of Hydrology 328: 511-22, doi: 10.1016/j.jhydrol.2005.12.011.

Werner, A. D. and M. R. Gallagher (2006). Characterisation of sea-water intrusion in the Pioneer Valley, Australia using hydrochemistry and three-dimensional numerical modelling. Hydrogeology Journal 14: 1452-1469, doi: 10.1007/s10040-006-0059-7.

Werner, A. D. and C. T. Simmons (2009). Impact of sea-level rise on sea water intrusion in coastal aquifers. Ground Water 47: 197-204, doi: 10.1111/j.1745-6584.2008.00535.x.

Werner, A. D., J. D. Ward, L. K. Morgan, C. T. Simmons, N. I. Robinson and M. D. Teubner (2012). Vulnerability indicators of sea water intrusion. Ground Water 50: 48-58, doi: 10.1111/j.1745-6584.2011.00817.x.

Werner, A. D., M. Bakker, V. E. A. Post, A. Vandenbohede, C. Lu and B. Ataie-Ashtiani (2013a). Seawater intrusion processes, investigation and management: Recent advances and future challenges. Advances in Water Resources 51: 3-26, doi: 10.1016/j.advwatres.2012.03.004.

Werner, A. D., Q. Zhang, L. Xue, B. D. Smerdon, X. Li, L. Yu and L. Li (2013b). An initial inventory and indexation of groundwater mega-depletion cases. Water Resources Management 27: 507-533, doi: 10.1007/s11269-012-0199-6.

Wu, J., Y. Xue, P. Liu, J. Wang, Q. Jiang and H. Shi (1993). Sea-water intrusion in the coastal Area of Laizhou Bay, China: 2. Sea-water intrusion monitoring. Ground Water 31: 740-745, doi: 10.1111/j.1745-6584.1993.tb00584.x.

Yakirevich, A., A. Melloul, S. Sorek, S. Shaath and V. Borisov (1998). Simulation of seawater intrusion into the Khan Yunis area of the Gaza Strip coastal aquifer. Hydrogeology Journal 6: 549-559, doi: 10.1007/s100400050175.

Figure Captions

Figure 1. Conceptual model of an unconfined coastal aquifer subjected to: (a) passive SWI, and (b) active SWI (modified after Badaruddin et al., 2015).

Figure 2. Estimation of T_i for the 5% relative salinity contour in the passive SWI (Case 1) and active SWI (Case 3) base cases.

Figure 3. Distribution of the 5% (black line), 50% (blue line) and 95% (red line) relative salinity contours at 0 y, 15 y and 30 y for: (a) passive SWI base case (Case 1), and (b) active SWI base case (Case 3).

Figure 4. Transient changes in SWI measurables. (a) Case 1 toe and tip position, (b) Case 3 toe and tip position, (c) Case 1 interface slope, (d) Case 3 interface slope, (e) Cases 1 and 3 mixing zone widths, and (f) Cases 1 and 3 freshwater discharge to the sea. In (a), (b) and (e), solid and dotted lines are the interface toe and tip, respectively. The black, blue and red lines in (a) to (d) are the 5%, 50% and 95% relative salinities.

Figure 5. Effects of different final boundary head differences ($h'_{f\text{-}s}$ of 0 m (black; Case 2), -1 m (green; Case 3) and -2 m (red; Case 4)) on active SWI: (a) tip and toe, (b) slope based on the 50% relative salinity contour, (c) interface width, and (d) seaward freshwater discharge. Solid and dashed lines in (a) and (c) are the interface toe and tip, respectively.

Figure 6. Distribution of the 5%, 50% and 95% relative salinity contours (solid lines) at 0 and 15 y using various values of: (a) hydraulic conductivity (Cases 7 and 11), and (b) porosity (Cases 39 and 43). Dashed lines represent salinity distributions of the active SWI base case.

Figure 7. Distribution of the 5%, 50% and 95% relative salinity contours at 0 and 15 y using various values of: (a) longitudinal dispersivity (Cases 15 and 19), and (b) aquifer thickness (Cases 31 and 35). Dashed lines represent salinity distributions of the active SWI base case.

Figure 8. Distribution of the 5%, 50% and 95% relative salinity contours at 0 and 15 y using various values of seawater density: (a) 1020 kg/m^3 (Case 23), and (b) 1030 kg/m^3 (Case 27). Dashed lines represent salinity distributions of the active SWI base case.

Figure 9. Scatter plot of the differences between the groundwater velocity (*v*) and the interface toe (□) and tip (+) in active SWI simulations. Black, blue and red symbols represent the cases with h'_{f-s} of 0, -1 and -2 m, respectively.

Figure 10. Linear regressions between $e^{h'_{f-s}}$ and T_i for: (a) the 5% relative salinity contour, (b) the 50% relative salinity contour, and (c) the 95% relative salinity contour, based on Cases 2 to 4 and 45 to 64.

Figure 11. Transient changes of: (a) interface locations, and (b) interface width, for Case 65. Solid and dotted lines represent the interface toe and tip, respectively.

Figure 12. Linear regressions between $e^{h'_{f-s}}$ and T_i for: (a) the 5% relative salinity contour, (b) the 50% relative salinity contour, and (c) the 95% relative salinity contour, in the field-scale cases.

Appendix A. The values of linear regression and determination coefficient in Figure 10

Figure	FHD Δh_f	Number of data points	a	b	R^2
(-)	m	(-)	(-)	(-)	(-)
	2.00	3	-0.10	10.7	0.99
	2.50	4	2.42	9.48	0.99
10a	3.00	5	2.62	9.67	0.99
	3.50	6	3.17	9.48	0.99
	4.00	6	3.94	8.99	0.99
	2.00	3	0.73	12.4	0.99
	2.50	4	2.48	11.7	0.99
10b	3.00	5	3.43	11.3	0.99
	3.50	6	3.96	11.1	0.99
	4.00	6	4.61	10.7	0.99
	2.00	3	-11.5	48.9	0.98
	2.50	4	-4.37	44.1	0.97
10c	3.00	5	-0.50	41.3	0.97
	3.50	6	1.74	39.7	0.97
	4.00	6	2.21	39.5	0.97

Appendix B. Passive SWI cases (at the initial steady-state and the second steady-state conditions after FHD)

Case	Initial θ (50% contour)	Final θ (50% contour)	Initial x_{toe} (50% contour)	Final x_{toe} (50% contour)	Initial W_{toe}	Final W_{toe}	Initial Pe	Final Pe	Initial MCR	Final MCR	Initial A_{SWI}	Final A_{SWI}	Initial Q_f	Final Q_f
1	9.240	4.290	169.0	386.2	31.50	130.2	0.009930	0.01034	0.06771	0.02486	0.000630	0.000251	0.54167	0.19265
5	9.240	4.290	169.0	386.2	31.50	130.2	0.009980	0.01047	0.06771	0.02325	0.000633	0.000254	0.27083	0.09635
9	9.240	4.290	169.0	386.2	31.50	130.2	0.009910	0.01027	0.06771	0.02486	0.000628	0.000249	1.08333	0.38537
13	8.310	3.530	198.6	470.5	8.000	45.00	0.001030	0.001154	0.06771	0.02486	0.0000660	0.0000280	0.54167	0.19268
17	17.20	9.540	92.50	186.5	94.50	183.0	0.09887	0.1021	0.06771	0.02486	0.00627	0.00248	0.54167	0.19273
21	12.23	5.760	131.5	292.5	21.40	81.00	0.009920	0.01032	0.08854	0.03471	0.000808	0.000346	0.56667	0.21521
25	8.050	3.440	208.5	490.5	44.50	193.0	0.009930	0.01035	0.05382	0.01829	0.000507	0.000186	0.51667	0.17016
29	9.710	4.790	140.2	286.7	27.20	79.20	0.01135	0.01184	0.06513	0.02886	0.000694	0.000332	0.45594	0.19480
33	9.120	3.730	190.1	475.2	34.50	187.4	0.008830	0.009170	0.06178	0.02254	0.000514	0.000202	0.55603	0.19719
37	9.240	4.290	169.0	386.2	31.50	130.2	0.009920	0.01031	0.06771	0.02486	0.000629	0.000250	0.54171	0.19270
41	9.240	4.290	169.0	386.2	31.50	130.2	0.009940	0.01036	0.06771	0.02486	0.000630	0.000251	0.54164	0.19260

Appendix C. Active SWI cases (at 15 y after FHD)

Case	θ (50% contour)	x_{toe} (95% contour)	x_{toe} (50% contour)	x_{toe} (5% contour)	x_{tip} (95% contour)	x_{tip} (50% contour)	x_{tip} (5% contour)	W_{toe}	W_{tip}	Pe	A_{SWI}	MCR	Q_f
2	4.110	280.2	410.6	450.4	0.0	0.0	27.80	170.2	27.80	0.01077	0.000159	0.01502	0.11265
3	3.460	373.3	547.5	611.3	31.50	59.20	165.8	238.0	134.3	0.01097	0.000584	0.05626	0.40790
4	3.890	481.1	692.8	778.8	203.6	273.4	479.8	297.7	276.2	0.01133	0.00102	0.09902	0.69314
6	7.990	183.2	210.2	290.8	0.0	0.0	10.60	107.6	10.60	0.01099	0.000163	0.01502	0.05634
7	4.750	265.2	375.0	412.8	0.0	8.800	30.60	147.6	28.60	0.01103	0.000588	0.05626	0.20395
8	4.720	384.5	495.0	612.1	140.0	150.3	346.6	227.6	206.6	0.01137	0.00102	0.09901	0.34657
10	3.620	372.0	502.5	645.8	0.00	36.00	58.10	273.8	58.10	0.01065	0.000158	0.01502	0.22523
11	3.120	470.4	730.2	825.2	124.9	184.5	410.0	354.8	285.1	0.01094	0.000583	0.05626	0.81581
12	4.100	580.3	823.2	993.1	270.0	470.5	668.1	412.8	398.1	0.01131	0.00102	0.09902	1.38634
14	3.660	436.0	460.7	492.8	0.0	0.0	13.80	56.80	13.80	0.001283	1.898E-5	0.01502	0.11262
15	2.700	578.6	650.7	665.5	15.30	25.60	49.10	86.90	33.90	0.001154	6.145E-5	0.05626	0.40792
16	2.620	730.1	800.7	876.9	167.0	177.0	240.0	146.8	73.80	0.001167	0.000105	0.09902	0.69319
18	6.070	40.00	282.8	320.6	0.0	5.000	226.1	280.6	226.1	0.1056	0.00156	0.01502	0.11262
19	11.28	140.1	362.8	530.8	74.60	214.9	461.4	390.6	386.8	0.1091	0.00581	0.05626	0.40785
20	45.71	237.3	452.8	723.9	226.0	425.0	710.2	486.6	484.2	0.1129	0.0102	0.09902	0.69315
22	4.350	251.2	387.8	394.2	0.0	0.0	20.00	143.0	20.00	0.01083	0.000160	0.01502	0.09009
23	3.840	347.3	497.8	552.3	34.90	58.10	155.1	205.0	120.1	0.01097	0.000684	0.06645	0.38538
24	4.100	460.0	687.8	720.5	207.1	290.2	447.0	260.5	234.0	0.01133	0.00121	0.1198	0.67065
26	3.630	307.2	464.8	508.5	0.0	0.0	31.00	201.3	31.00	0.01073	0.000159	0.01502	0.13514
27	3.160	397.2	594.8	668.6	30.30	61.00	182.0	271.3	151.7	0.01096	0.000517	0.04947	0.43043
28	3.180	502.1	814.8	836.0	203.4	301.0	512.0	333.9	308.6	0.01133	0.000890	0.08520	0.71569
30	4.130	240.2	360.0	390.0	0.0	0.0	21.00	150.0	21.00	0.01238	0.000225	0.01850	0.12025
31	3.520	313.2	470.0	534.2	30.00	51.00	160.0	221.0	130.0	0.01271	0.000810	0.06809	0.42555
32	3.740	418.4	650.0	688.4	205.2	268.0	425.2	270.0	220.0	0.01321	0.00142	0.1201	0.72082
34	3.990	310.3	480.0	520.3	0.0	0.0	31.00	210.0	31.00	0.009502	0.000141	0.01507	0.12813
35	3.390	431.3	610.0	680.3	35.1	62.00	159.1	249.0	124.0	0.009641	0.000492	0.05375	0.44344
36	3.720	514.6	817.5	854.6	200.0	302.0	500.0	340.0	300.0	0.009917	0.000849	0.09359	0.74873
38	3.590	337.5	480.0	537.5	0.0	10.00	35.00	200.0	35.00	0.01073	0.000159	0.01502	0.11268
39	3.380	426.5	634.0	715.5	65.20	100.0	271.2	288.5	206.0	0.01096	0.000584	0.05626	0.40792
40	3.400	543.0	750.0	888.0	270.5	355.0	600	345.0	329.5	0.01133	0.00102	0.09902	0.69317

42	7.670	200.0	219.0	315.0	0.0	0.0	15.0	115.0	15.0	0.01081	0.000160	0.01502	0.11262
43	4.270	332.6	482.0	535.6	10.0	25.0	60.0	203.0	50.0	0.01098	0.000585	0.05626	0.40788
44	3.260	436.3	510.0	696.3	159.0	213.0	384.0	260.0	225.0	0.01134	0.00102	0.09902	0.69312
45	3.380	337.1	503.4	562.3	0.0	4.0	45.0	225.2	45.0	0.01081	0.000411	0.03955	0.29167
46	4.840	235.0	336.5	363.2	0.0	0.0	12.2	128.2	12.2	0.01099	5.971E-5	0.00546	0.04167
47	5.090	232.5	331.5	356.5	0.0	0.0	12.0	124	12	0.01099	5.971E-5	0.00546	0.04167
48	4.220	275.4	400.0	438.2	0.0	0.0	26.0	162.8	26	0.01077	0.000159	0.01502	0.11265
49	3.550	325.3	478.0	530.1	0.0	3.0	39.0	204.8	39	0.01081	0.000411	0.03955	0.29167
50	3.400	385.5	572.6	644.2	39.00	68.0	194.3	258.7	155.3	0.01097	0.000584	0.05626	0.40790
51	3.530	437.5	645.0	728.6	125.0	179.7	367.5	291.1	242.5	0.01114	0.000898	0.08772	0.62500
52	5.140	230.0	328.0	352.5	0.0	0.0	12.6	122.5	12.6	0.01099	5.971E-5	0.00546	0.04167
53	4.290	272.0	393.5	431.0	0.0	0.0	25.3	159	25.3	0.01077	0.000159	0.01502	0.11265
54	3.640	319.8	466.5	516.0	0.0	3.0	37.5	196.2	37.5	0.01081	0.000411	0.03955	0.29167
55	3.790	494.0	718.5	814.0	217.5	288.0	515.0	320	297.5	0.01133	0.00102	0.09902	0.69314
56	5.000	229.5	326.0	350.7	0.0	0.0	12.7	121.2	12.7	0.01099	5.971E-5	0.00546	0.04167
57	4.180	269.2	391.0	426.5	0.0	0.0	24.3	157.3	24.3	0.01077	0.000159	0.01502	0.11265
58	3.740	315.5	459.6	508.3	0.0	1.0	36.5	192.8	36.5	0.01081	0.000411	0.03955	0.29167
59	3.460	367.0	535.5	597.4	28.00	47.0	144.1	230.4	116.1	0.01097	0.000584	0.05626	0.40790
60	5.030	228.5	324.0	349.0	0.0	0.0	11.5	120.5	11.5	0.01099	5.971E-5	0.00546	0.04167
61	4.210	268.0	387.5	424.0	0.0	0.0	23.4	156	23.4	0.01077	0.000159	0.01502	0.11265
62	3.780	313.2	456.4	504.0	0.0	2.0	35.5	190.8	35.5	0.01081	0.000411	0.03955	0.29167
63	3.530	363.0	528.0	588.5	25.00	45.0	135.0	225.5	110.0	0.01097	0.000584	0.05626	0.40790
64	3.610	418.5	606.7	678.5	108.0	154.5	317.0	260	209	0.01114	0.000898	0.08772	0.62500
65	9.210	1613	2700	3725	1517	2475	3625	2112	2108	0.08736	0.00311	0.03691	5.5455

Appendix D. The values of linear regression and determination coefficient in Figure 12

Figure	FHD Δh_f	Number of data points	a	b	R^2
(-)	m	(-)	(-)	(-)	(-)
12a	5.40	5	1.43	1.94	0.99
	5.80	5	1.78	1.68	0.99
	6.20	5	2.03	1.44	0.99
	6.60	5	2.25	1.20	0.99
	7.00	5	2.46	0.93	0.99
12b	5.40	5	2.43	5.35	0.99
	5.80	5	2.91	4.93	0.99
	6.20	5	3.18	4.61	0.99
	6.60	5	3.40	4.54	0.99
	7.00	5	3.75	4.13	0.99
12c	5.40	5	1.63	24.86	0.98
	5.80	5	1.90	24.53	0.98
	6.20	5	2.10	24.23	0.98
	6.60	5	2.34	24.16	0.98
	7.00	5	2.57	23.97	0.98